GEOPHYSICS, VOL. 77, NO. 6 (NOVEMBER-DECEMBER 2012); P. B253–B267, 12 FIGS., 1 TABLE.
10.1190/GEO2011-0515.1

Case History

Surface-downhole electrical resistivity tomography applied to monitoring of CO_2 storage at Ketzin, Germany

Peter Bergmann[1], Cornelia Schmidt-Hattenberger[1], Dana Kiessling[2], Carsten Rücker[3], Tim Labitzke[1], Jan Henninges[4], Gunther Baumann[4], and Hartmut Schütt[5]

ABSTRACT

Surface-downhole electrical resistivity tomography (SD-ERT) surveys were repeatedly carried out to image CO_2 injected at the pilot storage Ketzin, Germany. The experimental setup combines surface with downhole measurements by using a permanent electrode array that has been deployed in three wells. Two baseline experiments were performed during the site start-up and three repeat experiments were performed during the first year of CO_2 injection. By the time of the third repeat, approximately 13,500 tons of CO_2 had been injected into the reservoir sandstones at about 650 m depth. Field data and inverted resistivity models showed a resistivity increase over time at the CO_2 injector. The lateral extent of the related resistivity signature indicated a preferential CO_2 migration toward the northwest. Using an experimental resistivity-saturation relationship, we mapped CO_2 saturations by means of the resistivity index method. For the latest repeat, CO_2 saturations show values of up to 70% near the injection well, which matches well with CO_2 saturations determined from pulsed neutron-gamma logging. The presence of environmental noise, reservoir heterogeneities, and irregularities in the well completions are the main sources of uncertainty for the interpretations. The degradation of the permanently installed downhole components is monitored by means of frequently performed resistance checks. In consistency with the SD-ERT data, these resistance checks indicate a long-term resistivity increase near the CO_2 injector. In conclusion, the investigations demonstrate the capability of surface-downhole electrical resistivity tomography to image geologically stored CO_2 at the Ketzin site.

INTRODUCTION

The capture and storage of CO_2 in deep geologic formations is an option for reducing greenhouse gas emissions into the atmosphere (IPCC, 2005). Reliable long-term storage requires monitoring of CO_2 migration and related processes, e.g., brine displacement. In general, geophysical methods provide the images of physical parameters in regions of the subsurface that are otherwise inaccessible for direct observations. Time-lapse measurements allow for imaging of changes of these physical parameters over time, thus, offering an opportunity for long-term monitoring of CO_2 storage. Electrical resistivity tomography (ERT) is suitable in this context because the electric resistivity of porous sediments significantly increases when electrically conductive brine

Manuscript received by the Editor 19 December 2011; revised manuscript received 27 April 2012; published online 18 September 2012; corrected version published online 17 October 2012.
[1]GFZ German Research Centre for Geosciences, Helmholtz Centre Potsdam, Centre for CO_2 Storage, Potsdam, Germany. E-mail: bergmann@gfz-potsdam.de; conny@gfz-potsdam.de; labitzke@gfz-potsdam.de.
[2]University of Leipzig, Institute of Geophysics and Geology, Leipzig, Germany and GFZ German Research Centre for Geosciences, Helmholtz Centre Potsdam, Centre for CO_2 Storage, Potsdam, Germany. E-mail: dlaass@uni-leipzig.de.
[3]Technical University Berlin, Department of Applied Geophysics, Berlin, Germany. E-mail: carsten.ruecker@tu-berlin.de.
[4]GFZ German Research Centre for Geosciences, Helmholtz Centre Potsdam, Reservoir Technologies, Potsdam, Germany. E-mail: janhen@gfz-potsdam.de; gunther.baumann@gfz-potsdam.de.
[5]Formerly GFZ German Research Centre for Geosciences, Helmholtz Centre Potsdam, Centre for CO_2 Storage, Potsdam, Germany; presently Statoil ASA, Stavanger, Norway. E-mail: harsch@statoil.com.

is displaced by CO_2. Depending on the phase of the CO_2, dissolution in brine and uptake of dissolved solids can adversely decrease the resistivity. As an example for the reservoir conditions at the Ketzin site, laboratory data published by Fleury and Deschamps (2008) show that the effect of CO_2 dissolution on electrical brine conductivity — and therefore, bulk reservoir resistivity — is negligible. However, only short-term data are reported and, thus, additional physico-chemical fluid-solid interactions may affect the resistivity in the long-term.

Considering the rapid development of geoelectric instruments and inversion tools over the last few decades (e.g., Daily et al., 2004), ERT becomes an attractive monitoring option. The usefulness of time-lapse ERT is well documented, e.g., for steam injection (Ramirez et al., 1993), leak detection (Ramirez et al., 1996), salt tracer tracking (e.g., Slater et al., 2000; Kemna et al., 2002; Cassiani et al., 2006), and other processes related to subsurface fluid flow (LaBrecque et al., 2004; Nimmer et al., 2007; Clément et al., 2010). These applications are of high relevance for CO_2 storage monitoring because the methodical aspects and many practical problems are similar. Of special interest, however, are studies focused on the ERT imaging of subsurface CO_2 migration. Several modeling studies pointed out the potential for CO_2 storage monitoring by means of ERT (Ramirez et al., 2003; Christensen et al., 2006; al Hagrey, 2011). Practical application is being performed at the Nagaoka site in Japan (Xue et al., 2009; Nakatsuka et al., 2010), the SECARB Cranfield site in the USA (Carrigan et al., 2009), and the Ketzin site in Germany (Kiessling et al., 2010).

It is remarkable that most of these theoretical and practical studies deal with crosswell setups. This is because crosswell setups can be realized by permanent electrodes, which offer cost-competitive and environmentally sound long-term monitoring. In this article, we present the ERT surveys at the Ketzin site, which include a combination of well-based and surface-based data acquisition. Successful application of surface-based ERT for large- and midscale resistivity imaging are reported by Brunner et al. (1999), Storz et al. (2000), and Schütze et al. (2002). At the Ketzin site, large-scale geoelectrical measurements are adapted to the demand of high-resolution monitoring of the Ketzin storage reservoir by joint operation with a permanent borehole electrode array (Schmidt-Hattenberger et al., 2011, 2012), which allows for additional surface-downhole ERT (SD-ERT) data acquisition.

In this paper, we report the results of the SD-ERT surveys covering the startup of the Ketzin site and the first year of CO_2 injection by two baseline and three repeat surveys. The article is structured as followed: first, we give an overview on the Ketzin project and continue with the description of the SD-ERT surveys. We then describe the preprocessing and inversion of the field data. Subsequently, we estimate CO_2 saturations and compare them with results of pulsed-neutron-gamma logs. Finally, we discuss the value, implications, and limitations of SD-ERT for CO_2 plume tracking.

GEOELECTRICAL SURVEYING AT THE KETZIN SITE

Site description

The Ketzin project provides an experimental test site for the geologic storage of CO_2 in an onshore saline aquifer near Berlin (Schilling et al., 2009; Würdemann et al., 2010; Martens et al., 2011). Supercritical CO_2 is injected into Triassic sandstones of the Stuttgart Formation at approximately 650 m depth. Site operations were initiated by the CO_2SINK project in 2007, which was succeeded by the CO_2MAN project in 2010, both of which are here referred to as the Ketzin project. The objective of the Ketzin project is the improved understanding of in situ processes and the provision of practical experience for future geological storage of CO_2 (Giese et al., 2009). A primary task is the development and testing of geophysical monitoring procedures. Therefore, a wide range of activities is performed, such as active seismic experiments (e.g., Juhlin et al., 2007; Ivanova et al., 2012), combined active and passive seismic experiments (Arts et al., 2011), geoelectric experiments (Kiessling et al., 2010; Schmidt-Hattenberger et al., 2011), and electromagnetic experiments (Girard et al., 2011; Streich et al., 2011).

The Ketzin site is situated in the eastern part of the Roskow-Ketzin double anticline, which formed above a salt pillow situated at a depth of 1500–2000 m (Förster et al., 2006). One injection well (Ktzi201) and two observation wells (Ktzi200 and Ktzi202) have been drilled each to a depth of about 800 m. The wells are arranged in a rectangular triangle geometry (Figure 1a). All wells were drilled through the Stuttgart Formation, which is located in the depth range of about 630–700 m for the well Ktzi201. The Stuttgart Formation consists of sandstone channel-facies rocks with good reservoir properties alternating with muddy floodplain-facies rocks of poor reservoir quality (Förster et al., 2006; Norden et al., 2010). CO_2 has been injected into the saline-water-bearing sandstone units since 30 June 2008 via Ktzi201. The caprock overlying the Stuttgart Formation is the Weser Formation, which mainly consists of clayey and sandy siltstones alternating with carbonates and evaporites (Beutler and Nitsch, 2005). A high clay mineral content and the observed pore-space geometry make these rocks a suitable seal for the CO_2

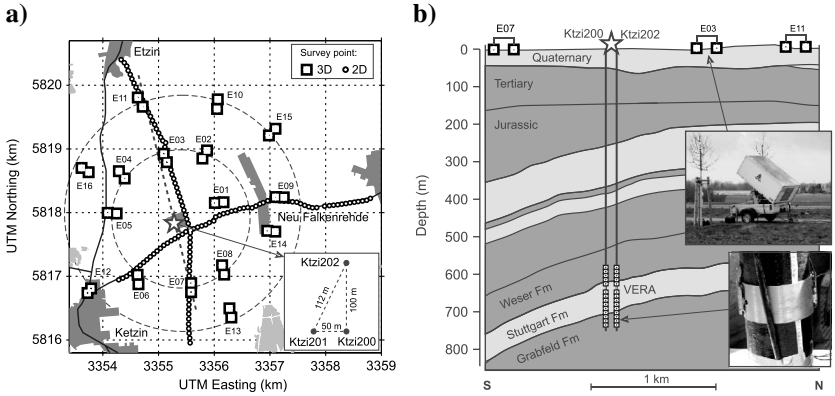

Figure 1. (a) Acquisition geometry for the SD-ERT. Surface dipoles E01-E08 are deployed on a circle with a radius of 800 m and surface dipoles E09-E16 are deployed on circle with a radius of 1500 m. Location of the injection site is shown by a star. (b) Schematic cross section through the Ketzin anticline and setup of the combined surface-downhole ERT experiments. Aquifer units are depicted in light gray, aquitard units in dark gray. The approximate position of the cross section is illustrated by a dotted line in the subfigure in (a). Upper inlay in (b) shows the TSQ-4 power source (property of Leipzig University). Lower inlay shows a VERA electrode mounted on the electrically insulated well pipe.

storage reservoir (Förster et al., 2006). A 10–20 m thick anhydrite layer, known as K2 (Keuper), outlines the top of the Weser Formation. The Weser Formation is overlain by mud/clay-carbonates of the Arnstadt Formation, which exhibits similar sealing properties. Until the year 2000, the shallower Hettangium formation (300–400 m) was used for industrial storage of natural gas (for further details, see Juhlin et al., 2007; Kazemenei et al., 2009).

Drilling operations started in summer 2007 with the sinking of the well Ktzi200. Well completion was performed with steel casings and preperforated screens in the reservoir zone (Prevedel et al., 2009).

A vertical electrical resistivity array (VERA) has been deployed in the three wells to allow for reservoir monitoring by means of geoelectric crosshole measurements. Each well hosts 15 electrodes, which are installed in the depth range 590 to 740 m with a vertical spacing of 10 m (Figure 2).

These electrodes consist of stainless steel rings that were mounted on the 5.5 inch casing strings. In the depth range of the electrodes, the casings were electrically insulated by an external coating that combines an epoxy matrix and a polyphenylene sulfide membrane (Kiessling et al., 2010). For connection of the electrodes to the surface, one multiconductor cable was used per well. To connect the individual electrodes to the cable, watertight cable outlets with watertight connectors have been realized (Schmidt-Hattenberger et al., 2011). Customized centralizers were deployed to center the strings inside the boreholes and protect the cables from mechanical damage. Mounting the electrodes and feeding the cables through the well head was performed during the well-completion operations and took about 24 hours per well (Prevedel et al., 2009). To prevent damage on the multiconductor cables the electric current passed through any two electrodes of the VERA is limited to 3 A (Kiessling et al., 2010).

A swellable packer was used for a staged cementation allowing the filter intervals to be excluded from the cementation. Thus, perforation of the steel casings was avoided that otherwise would have caused unmanageable risks of damaging the multiconductor cables (Prevedel et al., 2009). To eliminate the risk of clogging the preperforated filter screen, no such staged cementation was performed in Ktzi202 for the interval above the filters.

Injection of CO_2 started on 30 June 2008 with an average injection rate of about 3 tons/h for the first year. During this year, a total amount of about 17,900 metric tons of food-grade CO_2 has been injected through Ktzi201. Gas-chemical monitoring detected the arrival of CO_2 at the first observation well Ktzi200 (50 m away from Ktzi201) after about 530 tons of injected CO_2 on July 15th, 2008. Arrival at the second observation well Ktzi202 (112 m away from Ktzi201) was detected on 21 March 2009 after about 11,000 tons of CO_2 had been injected (Martens et al., 2011; Zimmer et al., 2011). The notable delay in the arrival at Ktzi202 is an indicator of the reservoir heterogeneity for which its channel-structure is likely to play a major role.

SD-ERT data collection

Geoelectric methods, alongside seismic methods and well logging, play an important role in the geophysical monitoring concept of the Ketzin site. Comprehensive CO_2 storage monitoring requires coverage at various temporal and spatial scales. All geophysical methods have their specific resolution, investigation depth, and sensitivity to reservoir properties. Therefore, geoelectric monitoring at Ketzin comprises the following three survey types to complement each other (Figure 1):

1) 3D SD-ERT: Current injection and voltage acquisition are performed at the surface using a sparse circular dipole geometry (surface-to-surface). Additional voltage acquisition is conducted in the three wells (surface-downhole) using the VERA system.
2) 2D SD-ERT: Current injection and voltage acquisition are performed by dipoles along two separate profiles that intersect near the injection location (surface-to-surface). Additional voltage acquisition is conducted in the well Ktzi201 (surface-downhole) using the VERA system. Two-dimensional SD-ERT surveys have been carried out exclusively in the CO_2 injection phase.
3) Crosshole ERT: Current injection and voltage acquisition are performed by the VERA system.

In the following section, we will concentrate on the 3D SD-ERT, which consists of 16 surface dipoles deployed on two concentric circles approximately centered on the injection location (Figure 1). The surface dipoles have a length of 150 m, are oriented toward the

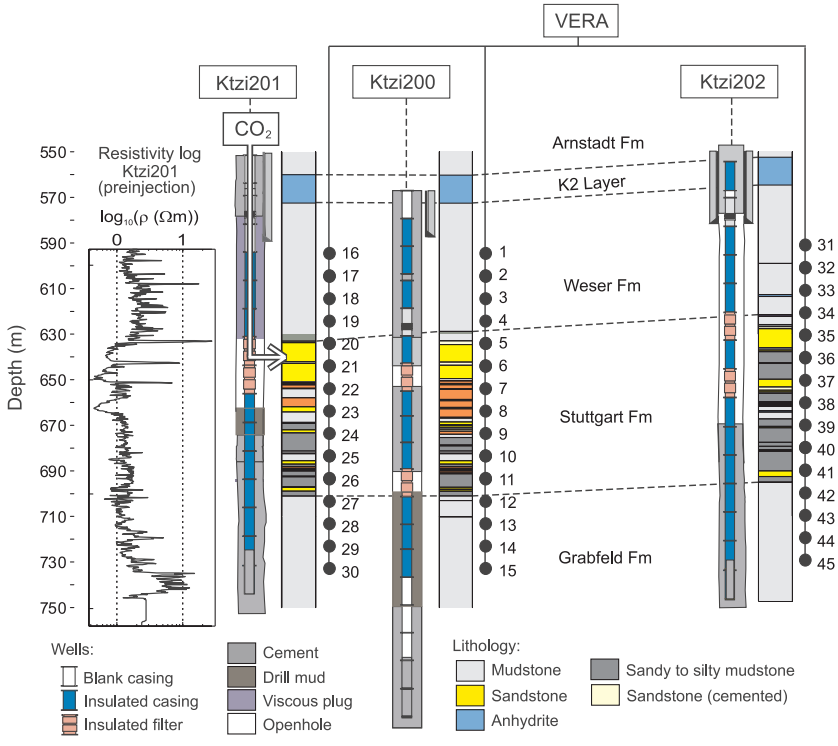

Figure 2. Well completion, lithology (after Förster et al., 2010) and electrode positions of the vertical electrical resistivity array (VERA) system (black dots) for the three wells at the Ketzin site. Ktzi201 is the injection well, Ktzi200 and Ktzi202 are observation wells. The left hand plot gives the logged resistivity for Ktzi201 acquired in the baseline period (after Norden et al., 2010).

injection site, and are used for current injection and for voltage acquisition. Current injection was performed by a TSQ-4 (Scintrex Limited, Canada) power source with a maximum power of 10 kW. Electrical currents of up to 11 A at a voltage of up to 3.3 kV were used. Injection was performed by a pulsed square-wave direct current (DC) with changing polarity (4s on +, 4s off, 4s on −, 4s off), with a signal period of 16 s. At each location, currents were injected for a period of approximately 45–60 minutes. These periods were divided into three intervals that were used for sequential voltage acquisition in the three wells. Voltage registration was realized by Texan-125 recorders (Refraction Technology Inc., USA). Survey crews typically consisted of five people and the surveys were usually completed within five working days.

The SD-ERT surveys were performed on a periodic basis and aligned to the arrival times of the CO_2 at the observation wells and operational circumstances (e.g., harvesting periods). The first baseline survey was performed in October 2007 and aimed to provide a noise test with full data acquisition. It showed a strong presence of environmental noise, with a particular source identified as pulsed electrical anticorrosion currents of a nearby gas pipeline. As an outcome of the noise analysis, the following surveys were performed within break periods that were arranged with the pipeline operator. A second baseline survey was carried out in April 2008 and showed an improved signal-to-noise ratio (S/N), which we will use as reference baseline. The first repeat survey was carried out in July 2008 after the detection of CO_2 at the first observation well Ktzi200. A second repeat survey was performed in November 2008 and a third repeat survey in April 2009 after CO_2 had been detected at the second observation well Ktzi202.

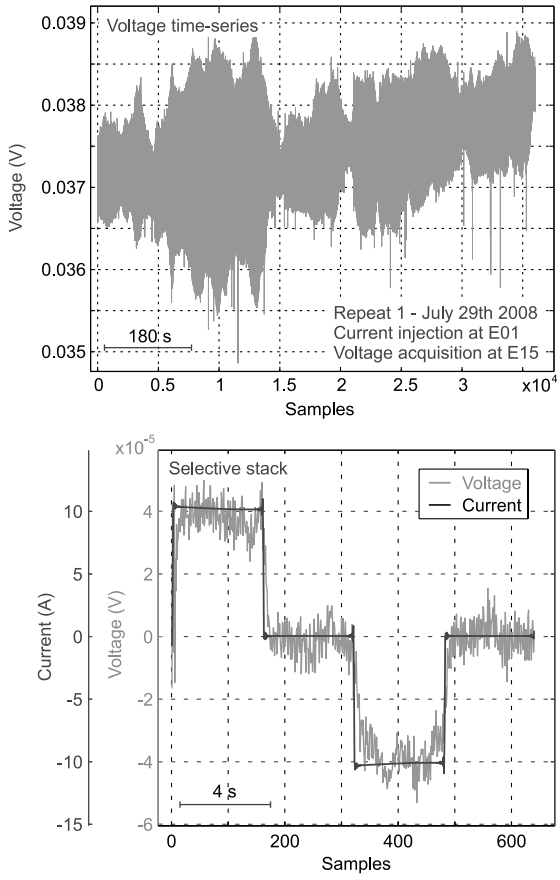

Figure 3. Example of a SD-ERT voltage time-series (top) and corresponding result after selective stacking (bottom).

ERT DATA PROCESSING

Preinversion processing

There are a number of infrastructural facilities near the Ketzin site that lead to a moderate S/N for the acquired voltage time series. Decentralized surface dipoles allowed to avoid long cable layouts that consequently reduced the risk of antenna effects and cable faults. However, significant noise remained and was addressed by a selective stacking approach after Storz et al. (2000). The approach aims to stack the acquired voltage time-series into single cycles and was implemented in the following steps:

1) noise removal (drift correction, despiking)
2) notch filtering (2.8 Hz, 8.4 Hz, and 16 Hz)
3) phase correction
4) alpha-trimmed median stack (10%)
5) windowing
6) determination of resistance and error

Phase correction was applied to align the voltage time-series to the respective current time-series. As the underlying crosscorrelation could easily produce sign switches, we continued with the absolute values of the apparent resistivities. Step four stacks the voltage time-series into 16 s cycles. The signal plateaus were then partitioned into time windows for identification of polarization asymptotes. Error values were estimated considering the voltage variation within the windows, as well as the voltage variation among the windows. Respecting the wide range of signal quality found in the stacked SD-ERT data, we estimate the average ratio of effective signal to effective noise to be about 10, which yields an average S/N of about 20 dB. An example of representative field data is given in Figure 3.

The pseudosections of the four SD-ERT surveys are shown in Figure 4. They allow for a first qualitative assessment with the following major findings: First, the best S/N can be found for the surface-downhole readings (Figure 4, upper part). Second, apparent resistivities obtained by current injection at the inner circle (Figure 4, abscissa E01-E08) are, on average, slightly higher than apparent resistivities with current injection at the outer circle (Figure 4, abscissa E09-E16). Third, an increase in resistivity over time can be seen for the electrodes that are deployed near the CO_2 injector in Ktzi201. Fourth, the third repeat shows an increase in resistivity for the Ktzi202 electrodes 31–34. Fifth, Ktzi202 electrodes 38–45 show remarkably low values. Sixth, Ktzi200 electrode 11 yields high apparent resistivities, which appears inconsistent with the adjacent electrodes.

Quality assessment by means of contact resistance checks

Operation of the VERA and electrode arrays at similar depths raises two questions: (1) Did any mechanical damage occur during the installation and (2) What is the operational lifetime?

The latter of these questions is determined by the reservoir conditions, which build an environment that is likely to cause metal corrosion and embrittlement of the nonmetallic cable elements, and is not yet conclusively assessable. To track the degradation of the subsurface electrodes, resistance checks were carried out

before and during the CO_2 injection. These checks measure the resistances between adjacent electrodes and use them simultaneously for currents and voltages. Therefore, these checks are more sensitive to the contact resistances than to reservoir resistivity and serve here as an indicator of the condition of the electrodes and materials in close contact (Figure 5). Resistance checks were first performed on a daily basis shortly before the start of the CO_2 injection, and continued with about one measurement per week since September 2008.

Figure 4 shows the conspicuous behavior of electrodes 39–45. In the following, we put some emphasis on them because they are an example for technical influences found in the SD-ERT data. The pseudosections show very low values for electrodes 39–45 (Figure 4), which seems to be confirmed by the rather low values found in the resistance checks (Figure 5). During the operation of the VERA system, we observed small amounts of brine at the surface termination of the multiconductor cable. Further investigation showed that this brine originated from the cable strands of electrodes 39–45. We suppose that the brine has penetrated the cable through a weakness of the insulation and has been moved upward by the subsurface overpressure. Figure 4 shows this behavior to be present from the beginning of the resistance checks. We consider it possible that the cable insulation has been mechanically damaged during the installation. An abrasion might have opened a pathway for the brine to enter the cable strands, which is plausible because the strands for electrodes 39–45 are placed adjacently within the cable. This damage is further supposed to be located between electrodes 38 and 39, ultimately disconnecting the deeper electrodes (>39). Subsequently, this could have created a short circuit, which would explain the low resistivities observed in the SD-ERT data and resistance checks. In conclusion, we decided the readings taken at electrodes 39–45, and for similar reasons, electrode 11, to be excluded from further processing.

Aside from these defects, the resistance checks allow us to draw some remarkable conclusions regarding resistivity increases found in the SD-ERT data. First, contact resistances and SD-ERT apparent resistivities display a steady increase for electrodes close to the CO_2 injection point (compare Figure 4 and Figure 5 at the arrows indicating the CO_2 injection). Both observations, although they reflect different effects (electrode degradation as opposed to a change in formation properties), are likely to be a consequence of the electrodes near the injection point coming into contact with the CO_2. Secondly, we find an abrupt increase in apparent resistivity at the Ktzi202 electrodes 31–34 (Figure 4). This increase appears with the third SD-ERT repeat survey, whereas the previous surveys indicated lower values at a relatively good repeatability. This abruptness becomes clearer in the resistance checks, which narrows the occurrence to the time interval 18–25 March 2009. This agrees with the chemically detected CO_2 arrival at this well on 21 March 2009.

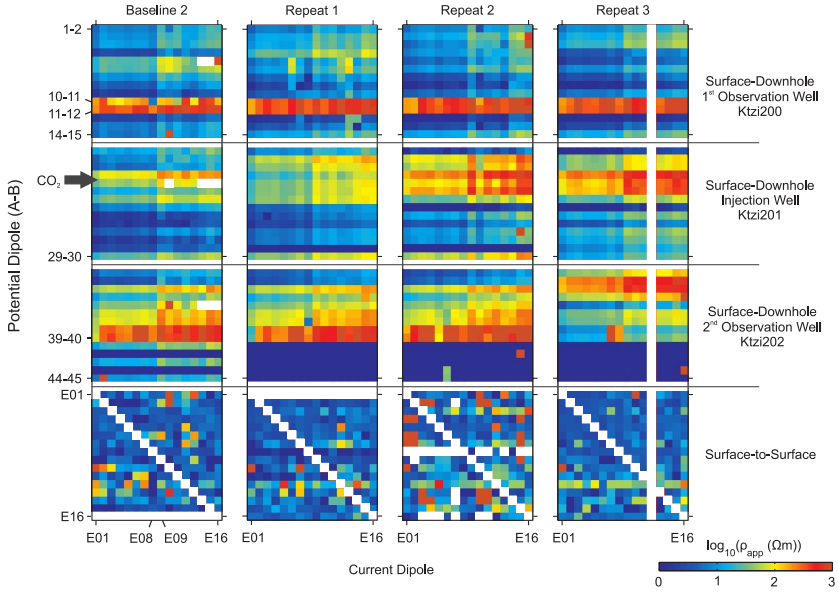

Figure 4. Pseudosections showing the apparent resistivities of the SD-ERT surveys. Abscissa shows the location of current injection at the surface dipoles E01-E16 (Figure 1). Ordinate shows the potential dipoles with the VERA electrodes 1–45 (Figure 2) and surface dipoles E01-E16.

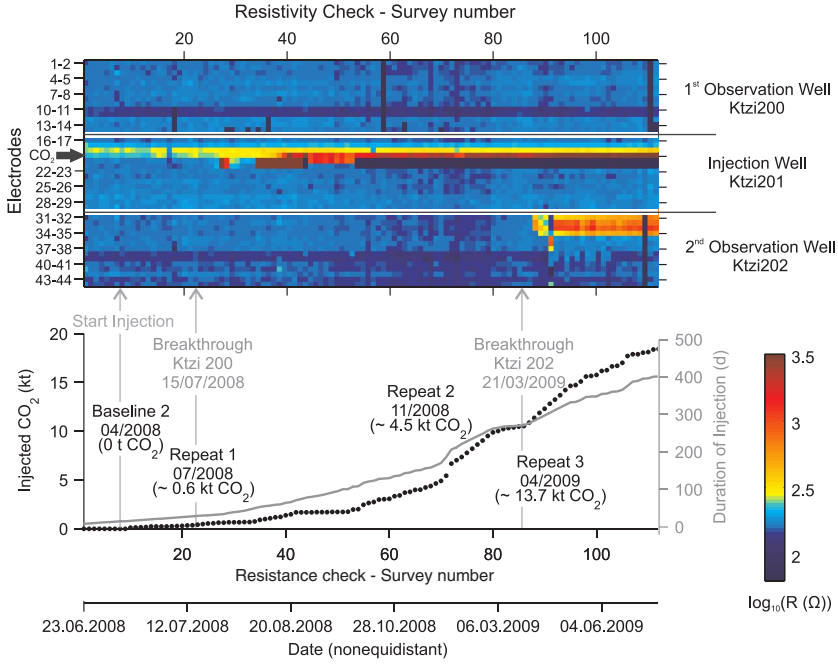

Figure 5. Resistance checks (upper plot) shown for the timeline of injection (lower plot). Black dots in time line indicate the cumulative mass of injected CO_2 (left ordinate), gray line shows the duration of injection in days (right ordinate). The lower plot is parameterized by the index of the resistivity check, which leads to a nonequidistant axis for the dates. Specific choice of the color map reveals that electrodes 11 and 39–45 are characterized by rather low resistances, presumably since the installation.

We have developed the following working hypothesis for this abrupt resistivity increase: Because there is no cementation in the interval above the filter screens of Ktzi202 (Figure 2), the arriving CO_2 displaced the brine in the annulus. This, in turn, caused the electrodes to lose contact with the formation, which the resistance checks indicate to have happened for electrodes 31–34 shortly before the third repeat survey. Further, we suppose the CO_2 uptake to have lasted a few weeks until having filled the annulus because the resistance checks stabilized at rather high levels within four to five measurement cycles (Figure 5).

ERT inversion

Given that the vertical spacing of the VERA electrodes is in the order of meters and the diameter of the outer electrode circle is in the order of kilometers, the volume to be inverted covers a range of scales. Thus, we required a nonequidistant parametrization to allow for efficient 3D inversions. To overcome these geometric constraints, we apply the triple-grid inversion technique (Günther et al., 2006) provided by the open-source software package BERT (boundless electrical resistivity tomography, www.resistivity.net). BERT combines a finite-element forward operator (Rücker et al., 2006) and a Gauss-Newton algorithm with inexact line search (Günther et al., 2006) and has been successfully applied in several case studies dealing with single-state, as well as time-lapse ERT data sets (e.g., Heincke et al., 2010; Coscia et al., 2011).

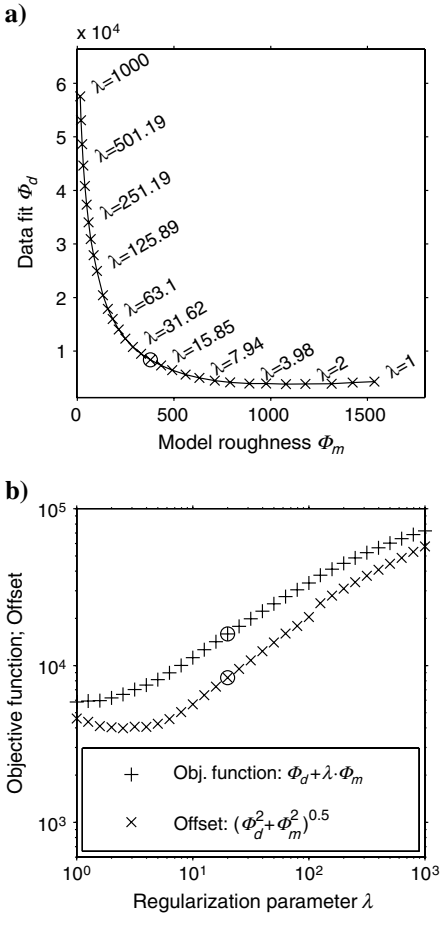

Figure 6. (a) An L-curve for the inversion of the second baseline data set and (b) L-curve parameters parameterized by the regularization. Circles indicate the solution for a regularization parameter of 20.

To define the inversion domain, we constructed a volume with a side length of 5 km and a depth of 2 km. This cube has then been populated with a parameter mesh of about 22,000 unstructured tetrahedral cells using the noncommercial mesh generator TetGen (Si, 2003). The resulting cell volumes were forced to be smallest near the electrodes and to coarsen toward the cube faces.

Inversion parameters have been determined successively by running inversions for which single parameters were varied. From these, we ascertain that the choices of the regularization parameter and the vertical roughness gradient weight have the largest impact on the inversion result. Large regularization parameters have the tendency to produce oversmoothed inversion results with poor data fits. Inversion with lower regularization parameters produce better data fits by means of increased model roughness. Finally, too weak regularizations generate mainly spurious structures. To foster the choice, we ran additional inversion sequences with variant regularization. From these, we selected a realization for which the inversion achieved an acceptable error, produced a result that is consistent with the preinversion data, and showed inverted resistivities to be stable for a relatively wide range of realizations. Following these criteria, we selected the regularization parameter equal to 20. We further assessed the choice of the regularization parameter by means of an L-curve analysis (Hansen and O'Leary, 1993; Figure 6). The inversion program aims to minimize the objective function which considers the data misfit Φ_d and the model misfit Φ_m (Günther et al., 2006). Contributions of both misfits to the objective function are balanced by the regularization parameter λ. A commonly used L-curve criterion suggests the optimum regularization parameter to be found where the offset of the function $\Phi_d(\Phi_m)$ to the origin is minimal (e.g., Aster et al., 2005). According to this criterion, we assess from Figure 6 a lower regularization parameter of about 2.5 to be justified as well. However, we retained a regularization parameter of 20 because that resulted in a better continuity in the time-lapse images (i.e., resistivity ratios). This, of course, leads to larger values for the objective function and χ^2 (final values are in the range of 4.7 to 7.8). Nevertheless, the relevant features in the resistivity images remain. The advantage of using stronger regularization is a better stability in the resistivity ratios. This is mainly due to the weakened impact of outliers, which can have a deteriorating impact when adverse perturbations occur in the numerators and denominators of the resistivity ratios.

In our case, these low fits are partly attributed to the heterogeneous coverage in the inversion volume. Large parts of the inversion volume are being poorly covered by the acquisition geometry. At some distance to the array, we do not expect to find a meaningful resistivity image. This is reflected in the fact that the low-coverage parts of the inversion volume do not show significant resistivity changes over time, which is principally acceptable.

The weight for vertical roughness gradients allows, to some extent, the incorporation of knowledge about the degree of geologic stratification. It can be used to stimulate an anisotropic appearance of the resulting resistivity image (e.g., Ellis and Oldenburg, 1994), which seems reasonable in view of the predominantly horizontal layering of the Ketzin reservoir. However, it will be shown later that the limited angle variation in the SD-ERT acquisition geometry causes a directional trend in the sensitivity patterns. In consequence,

the sensitivity patterns already inherit an emphasis of lateral structures in the inverted images. Because a further enhancement of this effect was not intended, we have opted for an almost isotropic roughness gradient. Although the code offers the definition of different regions with separate inversion parameters, we concentrated on selecting a set of global inversion parameters with respect to the reservoir geology. Inversion parameters are summarized in Table 1 and corresponding resistivity sections are shown in Figure 7 from which we make the following observations:

- Baseline 2: The east–west plane indicates a lower resistivity above and below the storage reservoir (Figure 7a). The north–south plane shows high resistances for Ktzi202 (at electrode 37), possibly extending into the reservoir (Figure 7b and 7c).
- Repeat 1: Figure 7c shows, compared with the baseline image, a rather similar resistivity in line with a slight resistivity decrease near the injector (Figure 7d).
- Repeat 2: A resistive structure appears centered at Ktzi201 near the injector (Figure 7g).
- Repeat 3: The resistive structure at Ktzi201 shows a more significant appearance (Figure 7j). A second strong resistivity increase appears at the upper electrodes of Ktzi202 (Figure 7k and 7l).

The model sensitivity, i.e., the Jacobi matrix containing the derivatives of the synthetic data with respect to changes in the model cell resistivities, was recalculated after each iteration, which was the most time consuming part of the inversion. The time-lapse procedure consists of taking the baseline resistivity inversion as the initial model for the subsequent repeats. The final baseline model was approached in five iterations, whereas the subsequent repeat models approached their final states after three to four iterations. As the number of iterations per repeat data set was not constant, we decided to keep the regularization fixed throughout the inversions. The initial model resistivity of the baseline was set to the median of the apparent resistivity of the field data, which is about 6.94 Ωm for the baseline data set.

We found that the incorporation of the data error, directly derived from the time-series, is not desirable for the temporal stability of the inversion results. After testing different error schemes, we decided to keep the data error as a threshold criterion for the individual readings. Unfortunately, due to the limited currents allowed for the borehole cables, it was not possible to realize reciprocal measurements, which could have been used for error estimation (e.g., Ramirez et al., 1996; LaBrecque et al., 2004). In consequence, we used an error estimation suggested by Friedel (2003). This error estimation is based on the minimum resolvable voltage U_{min}, which is to be known from equipment specifications and noise analysis of field data. Because the standard deviation usually increases as the measured voltage approaches U_{min}, readings become mainly random. This behavior is considered by an error drawn from the percentage ratio of the actual voltage and U_{min}, which is added to a percentage base-level error. Together with the data error drawn from the selective stacking and the electrode rejection based on the resistance checks, this estimated error is the third step in the data quality assessment.

INTERPRETATION

The resistivity increase at the injector is the most notable feature in Figure 7. This increase is generally consistent with the resistance checks, except for the resistivity decrease in repeat 1, for which we cannot provide a reasonable explanation yet. To the east, the resistivity increase can be traced to reach out to the observation well Ktzi200 (Figure 7g and 7h). To the west of Ktzi201 we find this signature to smear out, which indicates that it is somewhat less resolved outside the VERA.

The second resistive structure, appearing with the third repeat at Ktzi202, reflects the uptake of CO_2 into the uncemented annulus (Figure 7k and 7l). Because the annulus is a feature that is clearly below the resolution limit of the SD-ERT, we find its image as a spurious signature of increased resistivity in the formation.

Generally, the resistivity image is strongly affected by sensitivities that are related to the acquisition geometry. The typical sensitivity pattern of the SD-ERT arrangement is given in Figure 8a and appears as a tilted quadrupole with elongated cones. From this pattern, we find that the resolution is decreasing with distance to VERA electrodes, which makes imaging of thin-layered CO_2 migration at a distance of several electrode spacings unfeasible.

The data coverage is defined by the sum of the absolute sensitivities for all measurements (Figure 8b), and serves as a measure for the information content of the individual model cells. Due to the sparse surface-electrode arrangement, we can observe relatively

Table 1. Parameters for mesh definition and inversion.

Parameter	Setting	Remark
Mesh definition:		
Parameter mesh	5 km × 5 km × 2 km	Inversion domain
Secondary mesh	20 km × 20 km × 10 km	Forward modeling domain
Spatial growth rate of cells	1.12	BERT: Para3Dquality
Inversion:		
Regularization strength (λ)	20	
λ decrease	1	Constant regularization
Z weight	0.9	Almost isotropic
Lower/upper resistivity bound	0.1/2000 Ωm	

poor coverages in the volume overlying the VERA. As the region around the VERA electrodes shows the best coverage, it should yield the best resolution in the inversion image.

Impact of the large-scale heterogeneities and reservoir intercalations

By comparison of SD-ERT data with well-logged resistivities (Figure 2), we found two inconsistencies. First, SD-ERT resistivities (Figure 4) are, on average, one order of magnitude larger than logged resistivities. Second, the baseline SD-ERT (Figure 7a) shows the reservoir to be a zone of increased resistivity.

To understand these observations, we investigated a conceptual model comprising 15 electrodes situated in the subsurface and two current dipoles at the surface (Figure 9, left). The geometry was chosen to resemble the Ketzin SD-ERT setup with a single well. It further comprises the following elements: (a) a near-surface layer representing quaternary deposits, (b) a horizontal layer representing the K2 anhydrite, (c) a vertical layer embedding the well electrodes representing a simplified well completion, and (d) a layer of 2 m thickness representing a reservoir intercalation of cemented sandstone. The base model assumes a homogeneous resistivity of 2 Ωm for the background and all elements. Each of the subsequent resistivity modelings were conducted with one of the elements perturbed and compared against the results of the base model (Figure 9, right).

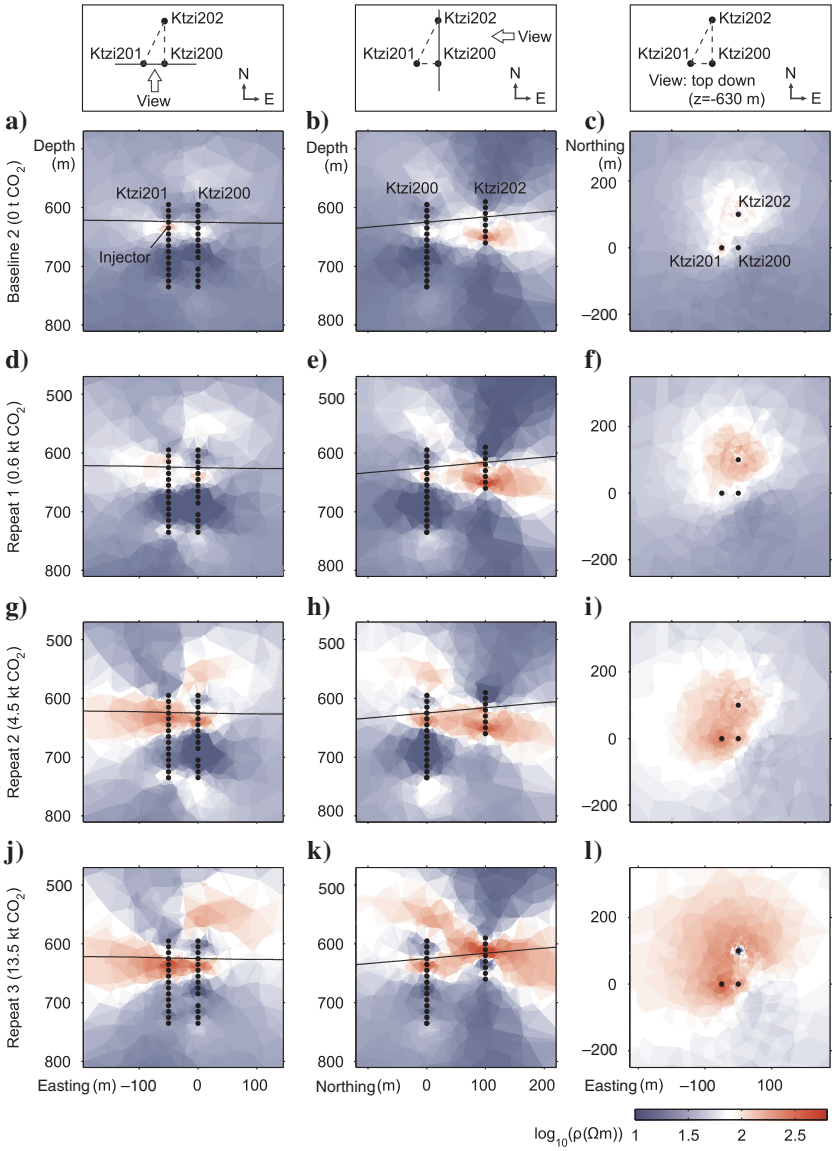

Figure 7. Inverted resistivity models for time-lapse SD-ERT data sets. The electrode next to the CO_2 injection is marked in (a). Black line shows the depth of top of the Stuttgart Formation as interpreted from seismic investigations (Juhlin et al., 2007). Easting and northing are referenced to Ktzi200. The main regions of resistivity increase are situated at the CO_2 injector (g and j) and in the upper part of Ktzi202 (k). The resistive zone at Ktzi202 is probably due to unsufficient contact of the respective electrodes to the formation (b, e, and h). Resistivity ratios for the observation plane Ktzi200/201 are given in Figure 11.

Model 1 investigates the impact of a near-surface layer that has its resistivity increased by a factor of 50. This factor was drawn from a short-spread resistivity survey, in which we found an average resistivity of about 100 Ωm up to a depth of 25 m. Corresponding synthetic apparent resistivities interestingly show a rather insignificant change. This lets us conclude that weathering-related moisture fluctuations in the near-surface might be of minor importance to the SD-ERT surveys, if they affect the surface dipoles equally. Model 2 incorporates a deeper layer that mimics the K2 anhydrites. It leads to a notable offset, shifting apparent resistivities toward smaller values. This offset seems to be increasing with decreasing distance between current injection and well head, and leads to a reduction of the apparent background resistivity by more than 50% in our model. The layer acts as a current barrier, which could be an explanation for the difference in SD-ERT resistivities with current injections performed at both circle radii.

The simplified well completion of model 3 assumes a homogeneous concrete column of 200 Ω m to be surrounding the electrodes. It leads to decreased resistivities at the top of the electrode array and slightly increased resistivities at the bottom. The effect is somewhat asymmetric with respect to the center of the downhole electrode arrangement and shows a magnitude of roughly −25%. However, the transferability of model 3 to the situation in Ketzin is limited due to the irregular completions of the Ketzin wells. We see a need for further investigation of completion-related effects following the approach of Doetsch et al. (2010). Effects of damages to the external coating of the steel casings, facilitating conductive coupling between the casing and the electrodes, need particular attention.

Model 4 incorporates a thin resistive layer between electrodes 4 and 5. This model addresses

reservoir intercalations of cemented sandstone of which at least three are present within the reservoir at Ktzi201 (Figure 2). Cemented layers of the reservoir sandstone act not only as relatively resistive intervals in the resistivity logs (Figure 2), but are also low-permeability constraints to the fluid migration (Wiese et al., 2010). Apparent resistivities of model 4 show a strong but highly localized increase with a maximum effect on the background resistivity of nearly +100% at the voltage dipole measuring across the layer. This, in turn, leads to the reservoir being imaged as an apparently resistive zone.

Although these models describe implications of resistive structures that can realistically be expected in the geologic setting of

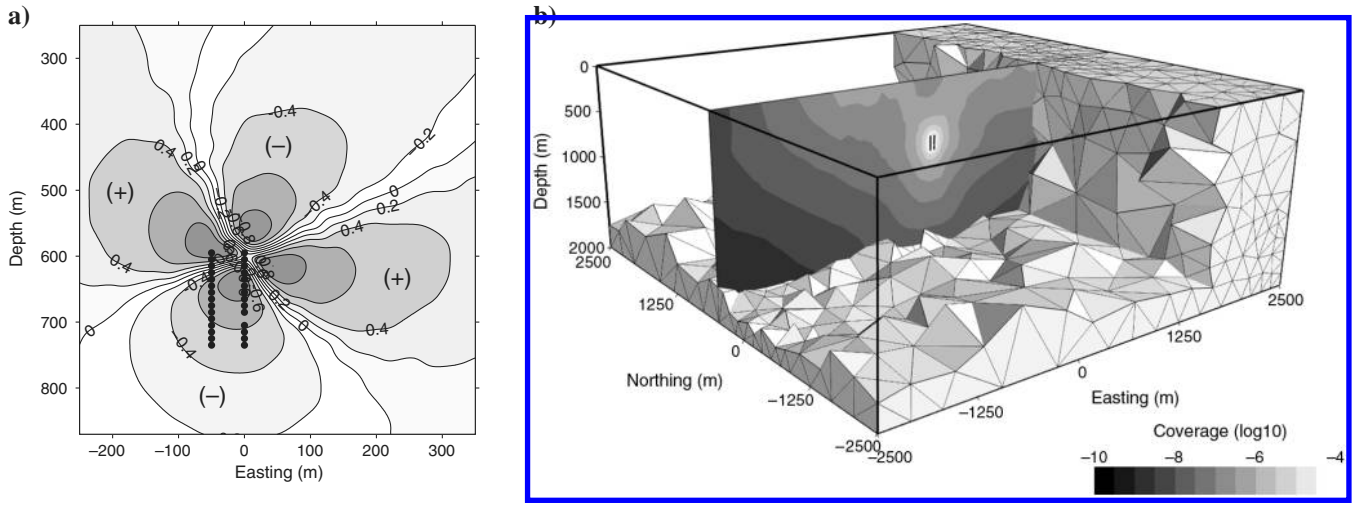

Figure 8. (a) Sensitivity pattern of a dipole-dipole SD-ERT measurement near the electrodes (black dots) of well Ktzi200 and Ktzi201. (b) Slice through the coverage volume embedded in the inversion mesh. The bright central part of the slice shows the highest coverage region near the VERA electrodes (black dots). Note that the average cell volumes decreases towards the VERA electrodes, to generate a low cell density at the boundary of the volume.

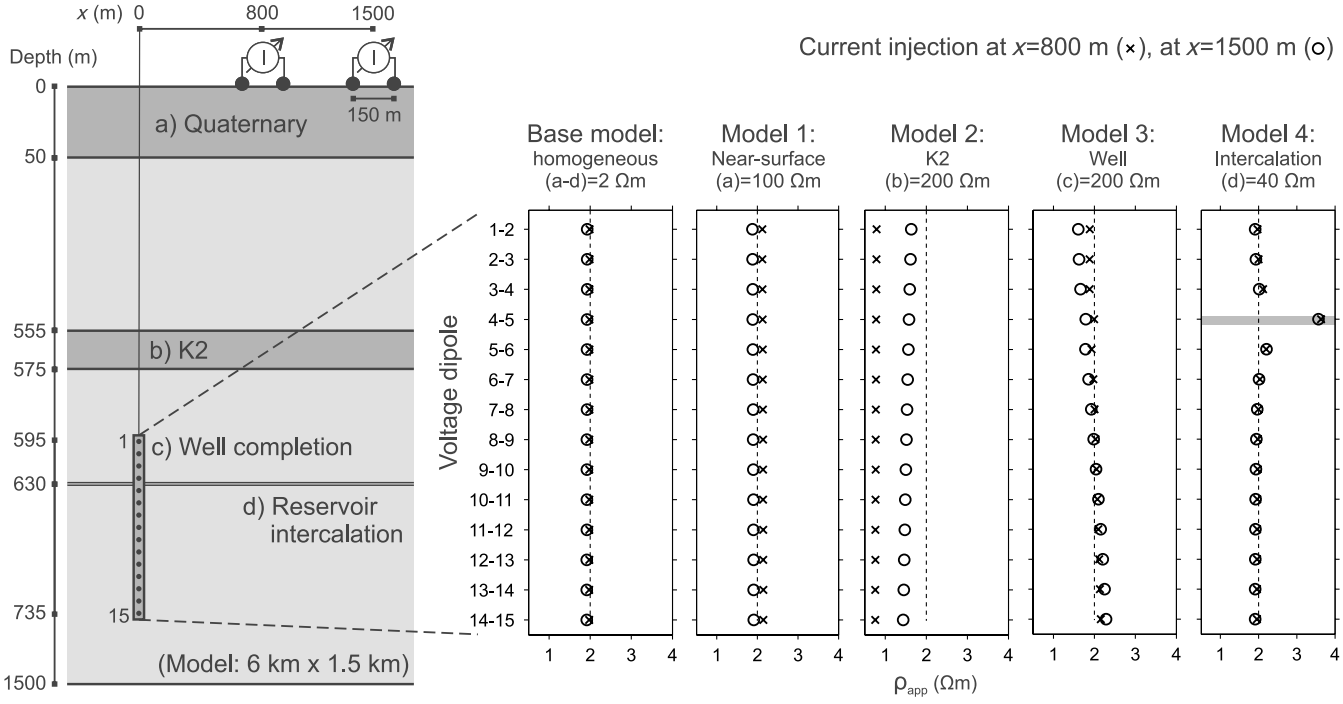

Figure 9. Left: Conceptual model comprising two current injections at the surface, 15 subsurface electrodes (black dots), and elements a–d used for resistivity modeling. Geometry is not drawn to scale. Right: Apparent resistivities from forward modeling. Gray bar in model 4 shows the voltage dipole which measures across the intercalation at a depth of 630 m.

the survey area, none of them can explain the consistently higher resistivity values compared to those found in the logs. We consider the likelihood that this observation is caused by the logging as rather low because the available logs are in good agreement, although being partly acquired by different logging operators. To evaluate potential technical reasons, we acquired additional SD-ERT data with different equipment, using a VIP10000 current transmitter (IRIS instruments) and Earth Data logger (GFZ Potsdam), but found a resistivity range that is consistent with our initial data. Thus, we consider it likely that the mismatch is a matter of the prospected scale and possibly anisotropy. There are, unfortunately, only a few references addressing the comparability of resistivity readings made on different spatial scales (e.g., Anderson et al., 1994; Jones, 1995; Aggelopoulos et al., 2005). However, it is widely accepted that there are scale-dependent effects involved when comparing data from well logs and surface-based surveys.

In the end, it is important to note that time-lapse application of SD-ERT surveying has the potential to reduce effects of static background heterogeneities.

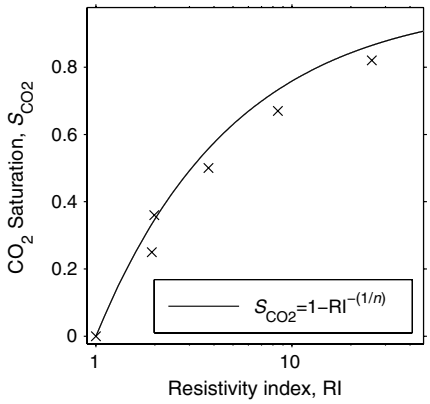

Figure 10. Resistivity index versus CO_2 saturation for the Ketzin reservoir sandstone modified after Kummerow and Spangenberg (2011). The solid line is plotted with $n = 1.62$.

CO_2 saturation estimation

Several petrophysical experiments have investigated the interdependence of CO_2 saturation and electric resistivity for the sandstones of the Ketzin reservoir (e.g., Schütt et al., 2005; Fleury et al., 2010; Zemke et al., 2010). Kummerow and Spangenberg (2011) constituted a relation between resistivity increase and saturation of pure CO_2 for the sandstone of the Ketzin reservoir (Figure 10), which will be used below.

Although the quantitative impact of the interfering effects is uncertain, we observe relative resistivity changes that appear consistent with these laboratory results. Thus, we use them to estimate the CO_2 saturation and subsequently conduct a validation with CO_2 saturations drawn from well logging. We follow the approach of Nakatsuka et al. (2010) by using the resistivity index (RI), i.e., the ratio of repeat resistivity and baseline resistivity. This approach requires no explicit knowledge about Archie parameters except for the saturation index n which is reported from laboratory experiments under in situ conditions to be about 1.62 (Kummerow and Spangenberg, 2011). Resistivity indexes and CO_2 saturation estimates for the observation plane Ktzi200/Ktzi201 are given in Figure 11.

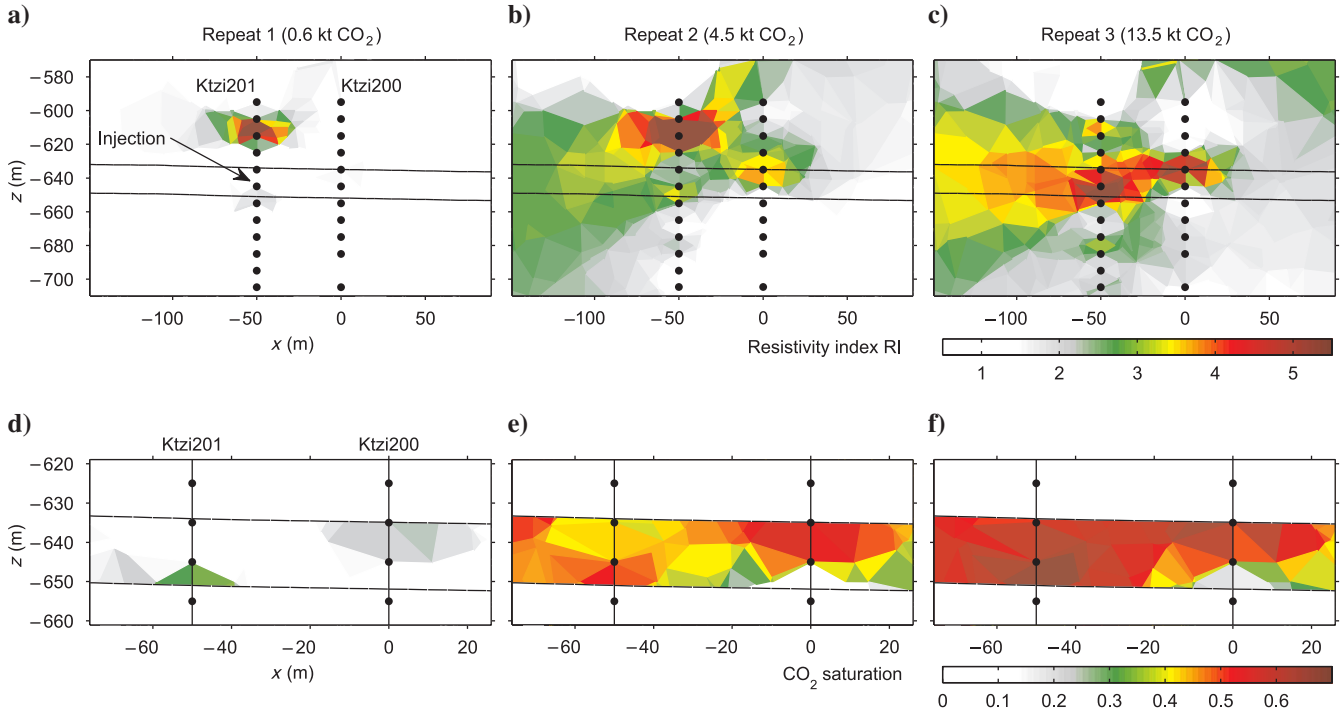

Figure 11. Resistivity index (top row) and estimated CO_2 saturation (bottom row) for the investigation plane Ktzi201/200. Dashed lines show the spatial extent of the reservoir sandstones schematically. CO_2 saturation estimation is constrained to the reservoir sandstones, for which the petrophysical relation given in Figure 10 was used.

The resistivity indexes given in Figure 11 show a dominant resistivity increase in the upper part of Ktzi201. This increase has a similar appearance as in Ktzi202 and, thus, might reflect problematic coupling conditions of the electrodes to the formation. Due to this similarity, we consider it likely that CO_2 penetrated into the well annulus of Ktzi201. We will return to this issue in the subsequent comparison with logging results. The third repeat interestingly shows this increase to diminish, and further, a notable

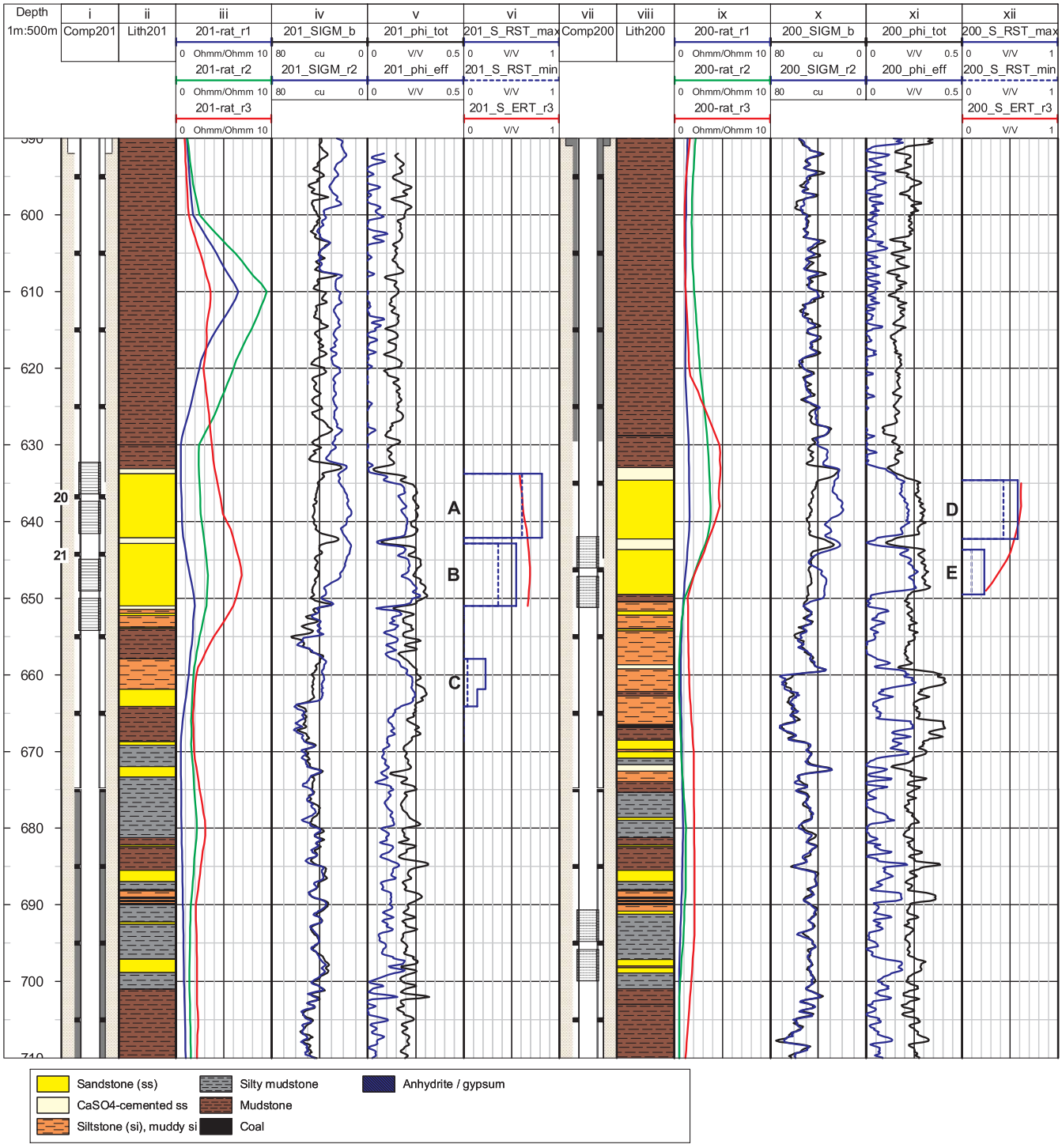

Figure 12. Comparison of CO_2 saturations derived from SD-ERT and pulsed neutron-gamma measurements for the injection well Ktzi201 (panels i–vi) and the observation well Ktzi200 (panels vii–xii). Panels show: Schematic well completion (i, vii), lithology after Förster et al. (2010) (ii, viii), resistivity ratio of baseline and repeated SD-ERT surveys (rat_r1, rat_r2, rat_r3 in iii, ix), SIGMA logs from baseline (b) and second repeat (r2) PNG runs (SIGM_b, SIGM_r2 in iv,x), porosities after Norden et al. (2010) (v, xi), and minimum and maximum scenario CO_2 saturations from PNG runs (S_RST_min, S_RST_max in vi, xii) overlain with the CO_2 saturations from the third SD-ERT repeat (S_ERT_r3 in vi, xii). VERA electrodes are shown by black symbols in the schematic well completions.

resistivity increase in the sandstone interval. Corresponding CO_2 saturations range from up to 30% for the first repeat, 30%–50% for the second repeat, to up to 70% for the third repeat.

Comparison with pulsed neutron-gamma logging

For a validation of the estimated CO_2 saturations, we compare them with results from time-lapse pulsed neutron-gamma (PNG) logging performed in the Ketzin wells. The PNG technique uses controlled neutron bursts that interact with the nuclei of the surrounding borehole and formation. After elastic and inelastic scattering, the neutrons are finally captured, mainly by hydrogen and chloride with a corresponding emission of gamma rays. The macroscopic capture cross section, SIGMA (Σ), is given in capture units (c.u.) and derives from the temporal decline of gamma rays. The high contrast of SIGMA between saline formation brine and gases makes the PNG technique well suited for detection of saturation changes during CO_2 injection in saline aquifers (Sakurai et al., 2005).

Baseline PNG logging was conducted on 9–10 June 2008, and several repeat logs were subsequently acquired. All of these logging runs were carried out with the Reservoir Saturation Tool (RST, Trademark of Schlumberger). For the purpose of this study, the second repeat run performed in June 2009 is evaluated because it is chronologically closest to the SD-ERT repeat 3. CO_2 saturations based on the PNG logs have been computed for a maximum scenario with standard environmental corrections and a minimum scenario using empirical corrections to consider the uncemented annuli. Details on the saturation calculations and corrections are given in Ivanova et al. (2012). Maximum and minimum scenario CO_2 saturations were averaged for a number of depth intervals that are compared against the CO_2 saturation estimates of the SD-ERT (Figure 12).

In the Ktzi201 and 200 wells (Figure 12), the main reservoir sandstone interval is separated by an intercalation of cemented sandstone at a depth of about 643 m (Norden et al., 2010). The intercalation is characterized by low porosities and low SIGMA values during the baseline RST run (Figure 12, iv and x), and separates the sandstone interval in an upper and a lower compartment (denoted as A/D and B/E, respectively, in Figure 12), both with a thickness of about 8–9 m.

For Ktzi201, PNG measurements yield CO_2 saturations of 61%–82% in the upper compartment (A), which compares to the range of 60%–70% estimated by the SD-ERT. In the lower compartment (B), PNG measurements yield CO_2 saturations in the range of 43%–58%. Corresponding CO_2 saturations based on SD-ERT are in the range of about 70%. Comparing the saturations derived from both methods, the SD-ERT appears to result in an overestimation here. In general, the SD-ERT indicates a major saturation increase to be situated within the lower compartment in contrast to the PNG logs, which indicate most significant saturations to occur in the upper compartment. This discrepancy may be due to the individual depth positions of the two electrodes (electrode 20 at 635 m depth and electrode 21 at 645 m depth) in the reservoir (Figure 12). We find electrode 21 to be situated relatively centered within the sandstone reservoir. Compared to that, we find electrode 20 at a short distance below the caprock, which produces weaker resistivity ratios than an electrode that is centered in the sandstone interval. We suppose that this is the reason for the smaller CO_2 saturation in the upper sandstone compartment compared to the lower compartment. There is a deeper interval in Ktzi201 (C) for which the PNG measurements yield CO_2 saturations in the range of 4%–23%. This interval is, however, not recognizable in the resistivity ratios. Because this can probably be attributed to the low thickness of this interval and the rather low CO_2 saturations at this depth, it gives some indication about the detection threshold provided by the SD-ERT.

In Figure 11, we observed a significant resistivity increase at Ktzi201 in the mudstone caprock at depths of about 600–630 m. The PNG SIGMA measurements show systematic offset of about 2.4–7 c.u. between the baseline and repeat measurements within the uncemented interval above the reservoir section of both wells (Ktzi201 and Ktzi202). This is interpreted as an effect related to a buoyancy-driven displacement of brine by CO_2 within these uncemented intervals of the well annuli because the otherwise required displacement within the mudstone caprock itself is physically not plausible at the given low effective porosities and permeabilities. The previous conclusions regarding the invasion of CO_2 into Ktzi201 and Ktzi202 are therefore confirmed by the PNG measurements.

For Ktzi200, we find PNG-based CO_2 saturations of 43%–58% in the upper sandstone compartment (D) and 10%–23% in the lower compartment (E), respectively. Although there is a reasonable match between the maximum values of the PNG logged CO_2 saturations and the saturations estimated from SD-ERT, we find the respective signature in the SD-ERT resistivity ratios to extend over a vertical distance of about 30 m (620–650 m). Under the assumption that the CO_2 in the upper compartment dominates the resistivity increase, the vertical extent of this resistivity increase might be an indicator for the relatively low vertical resolution. Accordingly, we estimate the SD-ERT to provide a vertical resolution of about three times the vertical electrode spacing. In contrast to that, vertical resolution and penetration depth of the PNG logs are in the order of a few decimeters. In consequence, it appears attractive to address future work on the calibration of ERT-based CO_2 saturations by the PNG measurements to gain saturation constraints at some distance to the wells.

CONCLUSIONS

This article presents the acquisition, inversion, and interpretation of the SD-ERT experiments that were conducted for monitoring of the Ketzin CO_2 storage pilot, Germany. We analyzed one baseline survey and three repeat surveys that were performed during the first year of site operation. Over the time of the three repeat surveys, the injected CO_2 amounted to 0.6 kt, 4.5 kt, and 13.5 kt, respectively. SD-ERT acquisitions were carried out in a dipole-dipole configuration with 16 current injections arranged on two concentric circles centered at the injection site. Current injections were performed at the surface with simultaneous voltage acquisition at the surface as well as downhole. Downhole voltages were measured using the VERA system, which provides 45 permanent electrodes within the injection well and two observation wells. Since the beginning of the CO_2 injection routine contact resistance checks are being carried out regularly to monitor the technical integrity of the VERA subsurface installations.

Inversion of the SD-ERT data was performed on an unstructured tetrahedral mesh, which was a crucial prerequisite for an efficient handling of the inverse problem. This applies in particular because the model, with a lateral extent of several kilometers, is required to incorporate the VERA electrodes that represent an arrangement

on the 1–10 m scale. As of the second repeat survey, the inverted models image an increase in resistivity around the CO_2 injector. An analysis of the lateral distribution of the resistivity increase indicates a preferential CO_2 migration in a northwesterly direction. We find a clear impact of the sensitivity patterns and consequential coverage in the resistivity images. There is a gradual decrease in sensitivity outside the VERA volume, leading to a rather low-resolved resistivity image at some distance to the wells.

We further used the imaged resistivity changes to estimate CO_2 saturations by means of the resistivity index method. This estimation was based on an established petrophysical relation, the Archie model, which was calibrated with lab data acquired under representative in situ conditions from the Ketzin reservoir sandstone. For the third repeat survey, estimated CO_2 saturations showed values of up to 70% near the injector, which was confirmed by a comparison with CO_2 saturations obtained independently from PNG logging.

Our investigations revealed the following three key issues concerning the reliability of the imaged resistivities. (1) The SD-ERT data showed a moderate S/N. This was addressed by sequential application of a selective stacking approach to the voltage time-series, contact resistance checks, and incorporation of error weights in the inversion. (2) The Ketzin reservoir is characterized by a rather pronounced heterogeneity and features several thin highly resistive layers of cemented sandstone. Due to their subhorizontal orientation, they cause apparently high resistivities in the SD-ERT image of the reservoir. The effects of selected background structures on the inversion results have been tested systematically with simple models. Time-lapse imaging has the potential to largely reduce effects of such background heterogeneities. (3) Realization of the Ketzin well completions was determined by the operational constraints. For instance, perforation of well casings after installation was not permitted due to uncontrollable risks for permanently installed inhole sensors. Therefore, a staged cementation procedure was conducted to prevent clogging of the preperforated filter-screens. In consequence, the Ketzin wells comprise uncemented intervals that produced significant time-lapse signals in the SD-ERT data when swept with CO_2. Thus, it was possible to identify time-lapse signatures in Ktzi201 and Ktzi202, which can likely be explained by CO_2 occupying these parts of the annuli. For a more detailed interpretation of the situation in Ktzi201, a comparison with PNG logs proved to be useful since providing information about the near-wellbore conditions.

We consequently underline three important aspects for practical realizations of deep ERT monitoring projects with downhole electrodes: (1) implementation of well completions that provide minimal irregularity, and (2) use of robust materials and installation designs that resist the corrosive environment in brine and CO_2 saturated reservoirs over the lifetime of the monitoring project. (3) We recommend additional quality controls for the electrodes, such as the described resistance checks.

Beside these technical results, our study has shown that imaging of CO_2 at the Ketzin site is possible by means of repeated SD-ERT surveys with a satisfactory resolution and sensitivity. A detailed analysis of the SD-ERT data sets showed not only its capability of detecting CO_2, but also, to some extent, reliable quantification of CO_2 saturations. With respect to our rather sparse survey layout, we see perspective improvement by the deployment of additional current dipoles, increased current dipole spacings, surface-downhole current injections, and electrode installations in potentially deviated wells.

Due to the abundance of aspects for the crosswell ERT surveys, it was not possible to give a comparison with the SD-ERT already here. It is, however, worth noting that surface-downhole surveying is a particular option for situations where broad azimuth coverage is demanded or only single wells are available. The use of permanently installed downhole electrodes proved to be crucial to achieve sufficient coverage and resolution at the target reservoir. Furthermore, the VERA realization of such electrodes at the Ketzin site has proved to offer diverse opportunities for alternative geoelectric and electromagnetic surveys. In this regard, we see a promising perspective in the collaboration of frequently repeated crosshole ERT and periodical SD-ERT. Moreover, there is multiple potential for integration of SD-ERT results with other monitoring methods. In this context, we will address continuing investigations on a combined interpretation with the time-lapse seismic data acquired at the Ketzin site, as well as the incorporation of seismic structural constraints into the SD-ERT inversion.

Based on the presented outcomes and the practical experience gained at the Ketzin site, we consider SD-ERT as a promising method that can contribute to monitoring of CO_2 storages within a suite of geophysical methods. Finally, there is a potential for SD-ERT to be an easily applicable supplement to borehole ERT, which is also of interest for monitoring of other subsurface fluid migration processes that lead to sufficient resistivity changes.

DATA ACCESS

The presented SD-ERT data can be retrieved from doi: 10.5880/GFZ.b103-12051.1 and further technical descriptions at Labitzke et al. (2012). Here, one will find the raw field data (voltage time-series), the preprocessed data (apparent resistivities), and the scripts that were used for processing and inversion of the data.

ACKNOWLEDGMENTS

We express thanks to the landowners for permitting access to their properties. We are also grateful to the many people involved in the surveys, in particular Erik Danckwardt, Roland Hohberg, Martin Seidel, Günter Petzold, Marco Pohle, and René Voigt of Leipzig University. Kay Krüger (GFZ) is acknowledged for valuable technical comments and Birgit Schöbel (GFZ) for support in operational and logistic matters. Dat Vu-Hoang and Karl Schwab (Schlumberger) are acknowledged for their cooperation on the interpretation of the PNG logging data. We thank the reviewers (Oliver Kuras and two anonymous reviewers) for their constructive criticism that helped to improve this paper.

We would like to thank all partners of the Ketzin project for their continued support and contributions. The project CO_2SINK and its follow-up CO_2MAN receive their funding from the European Commission (Sixth Framework Program, FP6), two German ministries — the Federal Ministry of Economics and Technology (COORETEC Program) and the Federal Ministry of Education and Research (GEOTECHNOLOGIEN Program) — as well as from industry partners. We acknowledge the COSMOS project for funding the VERA system. The first author would like to thank the GeoEn project (Grant 03G0671A/B/C), a national scientific initiative in the field of energy research.

REFERENCES

Aggelopoulosa, C., P. Klepetsanisa, M. A. Theodoropouloub, K. Pomonic, and C. D. Tsakiroglou, 2005, Large-scale effects on resistivity index of porous media: Journal of Contaminant Hydrology, **77**, 299–323, doi: 10.1016/j.jconhyd.2005.02.002.

al Hagrey, S. A., 2011, 2D optimized electrode arrays for borehole resistivity tomography and CO_2 sequestration modelling: Pure and Applied Geophysics, 1–10, doi: 10.1007/s00024-011-0369-0.

Anderson, B., I. Bryant, M. Lülig, B. Spies, and K. Helbig, 1994, Oilfield anisotropy: Its origins and electrical characteristics: Oilfield Review, **6**, no. 4, 48–56.

Arts, R., J. Meekes, J. Brouwer, M. van der Werf, R. Noorlandt, B. Paap, W. Visser, V. Vandeweijer, S. Lüth, R. Giese, and J. Maas, 2011, Results of a monitoring pilot with a permanent buried multicomponent seismic array at Ketzin: Energy Procedia, **4**, 3588–3595, doi: 10.1016/j.egypro.2011.02.288.

Aster, R. C., C. H. Thurber, and B. Borchers, 2005, Parameter estimation and inverse problems: Academic Press Inc.

Beutler, G., and E. Nitsch, 2005, Paläographischer Überblick, *in* G. Beutler, N. Hauschke, E. Nitsch, and U. Vath, eds., Stratigraphie von Deutschland IV, Keuper: Courier Forschungsinstitut Senckenberg, 253, 15–30.

Brunner, I., S. Friedel, F. Jacobs, and E. Danckwardt, 1999, Investigation of a tertiary maar structure using 3-D resistivity imaging: Geophysical Journal International, **136**, 771–780, doi: 10.1046/j.1365-246x.1999.00770.x.

Carrigan, C. R., A. L. Ramirez, R. L. Newmark, R. Aines, and S. J. Friedmann, 2009, Application of ERT for tracking CO_2 plume growth and movement at the SECARB Cranfield site: Presented at the 8th Annual Conference on Carbon Capture and Sequestration.

Cassiani, G., V. Bruno, A. Villa, N. Fusi, and A. M. Binley, 2006, A saline trace test monitored via time-lapse surface electrical resistivity tomography: Journal of Applied Geophysics, **59**, 244–259, doi: 10.1016/j.jappgeo.2005.10.007.

Christensen, N. B., D. Sherlock, and K. Dodds, 2006, Monitoring CO_2 injection with crosshole electrical resistivity tomography: Exploration Geophysics, **37**, 38–42, doi: 10.1071/EG06044.

Clément, R., M. Descloitres, T. Günther, L. Oxarango, C. Morra, J.-P. Laurent, and J.-P. Gourc, 2010, Improvement of electrical resistivity tomography for leachate injection monitoring: Waste Management, **30**, 452–464, doi: 10.1016/j.wasman.2009.10.002.

Coscia, I., S. A. Greenhalgh, N. Linde, J. Doetsch, L. Marescot, T. Günther, T. Vogt, and A. G. Green, 2011, 3D crosshole ERT for aquifer characterization and monitoring of infiltrating river water: Geophysics, **76**, no. 2, G49–G59, doi: 10.1190/1.3553003.

Daily, W., A. Ramirez, A. Binley, and D. LaBrecque, 2004, Electrical resistance tomography: The Leading Edge, **23**, 438–442, doi: 10.1190/1.1729225.

Doetsch, J. A., I. Coscia, S. A. Greenhalgh, N. Linde, A. G. Green, and T. Günther, 2010, The borehole-fluid effect in electrical resistivity imaging: Geophysics, **75**, no. 4, F107–F114, doi: 10.1190/1.3467824.

Ellis, R., and D. Oldenburg, 1994, Applied geophysical inversion: Geophysical Journal International, **116**, 5–11, doi: 10.1111/gji.1994.116.issue-1.

Fleury, M., and H. Deschamps, 2008, Electrical conductivity and viscosity of aqueous NaCl solutions with dissolved CO_2: Journal of Chemical and Engineering Data, **53**, 2505–2509, doi: 10.1021/je8002628.

Fleury, M., S. Gautier, N. Gland, P. Boulin, B. Norden, and C. Schmidt-Hattenberger, 2010, Petrophysical measurements for CO_2 storage: Application to the Ketzin site: International Symposium of the Society of Core Analysts, SCA2010-06, p. 12.

Förster, A., B. Norden, K. Zinck-Jørgensen, P. Frykman, J. Kulenkampff, E. Spangenberg, J. Erzinger, M. Zimmer, J. Kopp, G. Borm, C. Juhlin, C. Cosma, and S. Hurter, 2006, Baseline characterization of the CO_2SINK geological storage site at Ketzin, Germany: Environmental Geosciences, **13**, 3, 145–161, doi: 10.1306/eg.02080605016.

Förster, A., R. Schöner, H.-J. Förster, B. Norden, A.-W. Blaschke, J. Luckert, G. Beutler, R. Gaupp, and D. Rehde, 2010, Reservoir characterization of a CO_2 storage aquifer: The upper Triassic Stuttgart Formation in the northeast German Basin: Marine and Petroleum Geology, **27**, 2156–2172, doi: 10.1016/j.marpetgeo.2010.07.010.

Friedel, S., 2003, Resolution, stability and efficiency of resistivity tomography estimated from a generalized inverse approach: Geophysical Journal International, **153**, 305–316, doi: 10.1046/j.1365-246X.2003.01890.x.

Giese, R., J. Henninges, S. Lüth, D. Morozova, C. Schmidt-Hattenberger, H. Würdemann, M. Zimmer, C. Cosma, and Ch. Juhlin, CO_2SINK Group 2009, Monitoring at the CO_2SINK site: A concept integrating geophysics, geochemistry and microbiology: Energy Procedia, **1**, 2251–2259, doi: 10.1016/j.egypro.2009.01.293.

Girard, J. F., N. Coppo, J. Rohmer, B. Bourgeois, V. Naudet, and C. Schmidt-Hattenberger, 2011, Time-lapse CSEM monitoring of the Ketzin (Germany) CO_2 injection using 2 MAM configuration: Energy Procedia, **4**, 3322–3329, doi: 10.1016/j.egypro.2011.02.253.

Günther, T., C. Rücker, and K. Spitzer, 2006, Three-dimensional modelling and inversion of DC resistivity data incorporating topography II. Inversion: Geophysical Journal International, **166**, 506–517, doi: 10.1111/gji.2006.166.issue-2.

Hansen, P. C., and D. P. O'Leary, 1993, The use of the L-curve in the regularization of discrete ill-posed problems: SIAM Journal on Scientific Computing, **14**, 1487–1503, doi: 10.1137/0914086.

Heincke, B., T. Günther, E. Dahlsegg, J. S. Rønning, G. Ganerød, and H. Elvebakk, 2010, Combined three-dimensional electric and seismic tomography study on the Åknes rockslide in western Norway: Journal of Applied Geophysics, **70**, no. 4, 292–306, doi: 10.1016/j.jappgeo.2009.12.004.

IPCC, B. Metz, O. Davidson, H. C. de Coninck, M. Loos, and L. Meyer, eds., 2005, IPCC special report on carbon dioxide capture and storage: Working group III of the intergovernmental panel on climate change: Cambridge University Press.

Ivanova, A., A. Kashubin, N. Juhonjuntti, J. Kummerow, J. Henninges, Ch. Juhlin, S. Lüth, and M. Ivandic, 2012, Monitoring and volumetric estimation of injected CO_2 using 4D seismic, petrophysical data, core measurements and well logging: A case study at Ketzin, Germany: Geophysical Prospecting, **60**, 957–973, doi:10.1111/j.1365-2478.2012.01045.x.

Jones, J. W., 1995, Scale-dependent resistivity measurements of Oracle granite: Geophysical Research Letters, **22**, 1453–1456, doi: 10.1029/95GL01495.

Juhlin, C., R. Giese, K. Zinck-Jørgensen, C. Cosma, H. Kazemeini, N. Juhojuntti, S. Lüth, B. Norden, and A. Förster, 2007, 3D baseline seismics at Ketzin, Germany: The CO_2SINK project: Geophysics, **72**, no. 5, B121–132, doi: 10.1190/1.2754667.

Kazemeini, S. H., C. Juhlin, K. Zinck-Jørgensen, and B. Norden, 2009, Application of the continuous wavelet transform on seismic data for mapping of channel deposits and gas detection at the CO_2SINK site, Ketzin, Germany: Geophysical Prospecting, **57**, 111–123, doi: 10.1111/gpr.2008.57.issue-1.

Kemna, A., B. Kulessa, and H. Vereecken, 2002, Imaging and characterisation of subsurface solute transport using electrical resistivity tomography (ERT) and equivalent transport models: Journal of Hydrology, **267**, 125–146, doi: 10.1016/S0022-1694(02)00145-2.

Kiessling, D., C. Schmidt-Hattenberger, H. Schütt, F. Schilling, K. Krüger, B. Schöbel, E. Danckwardt, and J. Kummerow, the CO_2SINK Group, 2010, Geoelectrical methods for monitoring geological CO_2 storage: First results from cross-hole and surface-downhole measurements from the CO_2SINK test site at Ketzin (Germany): International Journal of Greenhouse Gas Control, **4**, 816–826, doi: 10.1016/j.ijggc.2012.05.001.

Kummerow, J., and E. Spangenberg, 2011, Experimental evaluation of the impact of the interactions of $CO_2 - SO_2$, brine, and reservoir rock on petrophysical properties: A case study from the Ketzin test site, Germany: Geochemistry Geophysics Geosystems, **12**, Q05010, doi: 10.1029/2012GC003469.

Labitzke, T., P. Bergmann, D. Kiessling, and C. Schmidt-Hattenberger, 2012, 3D surface-downhole electrical resistivity tomography data sets of the Ketzin CO_2 storage pilot from the CO_2SINK project phase: Scientific Technical Report — Data, 12/05, doi: 10.2312/GFZ.b103-12051.

LaBrecque, D. J., G. Heath, R. Sharpe, and R. Versteeg, 2004, Autonomous monitoring of fluid movement using 3D electrical resistivity tomography: Journal of Environmental and Engineering Geophysics, **9**, no. 3, 167–176, doi: 10.4133/JEEG9.3.167.

Martens, S., A. Liebscher, F. Möller, H. Würdemann, F. Schilling, and M. Kühn, , Ketzin Group, 2011, Progress report on the first European onshore CO_2 storage site at Ketzin (Germany) — Second year of injection: Energy Procedia, **4**, 3246–3253, doi: 10.1016/j.egypro.2011.02.243.

Nakatsuka, Y., Z. Xue, H. Garcia, and T. Matsuoka, 2010, Experimental study on CO_2 monitoring and quantification of stored CO_2 in saline formations using resistivity measurements: International Journal of Greenhouse Gas Control, 4, 209–216, doi: 10.1016/j.ijggc.2010.01.001.

Nimmer, R. E., J. L. Osiensky, A. M. Binley, K. F. Sprenke, and B. C. Williams, 2007, Electrical resistivity imaging of conductive plume dilution in fractured rock: Hydrogeology Journal, **15**, 877–890, doi: 10.1007/s10040-007-0159-z.

Norden, B., A. Förster, D. Vu-Hoang, F. Marcelis, N. Springer, and I. Le Nir, 2010, Lithological and petrophysical core-log interpretation in CO_2SINK, The European onshore research storage and verification project: SPE Reservoir Evaluation and Engineering, **13**, 179–192, doi: 10.2118/115247-PA.

Prevedel, B., L. Wohlgemuth, B. Legarth, J. Henninges, H. Schütt, C. Schmidt-Hattenberger, B. Norden, A. Förster, and S. Hurter, 2009, The CO_2SINK boreholes for geological CO_2-storage testing: Energy Procedia, **1**, 2087–2094.

Ramirez, A., W. Daily, A. Binley, D. LaBrecque, and D. Roelant, 1996, Detection of leaks in underground storage tanks using electrical resistance

methods: Journal of Environmental and Engineering Geophysics, **1**, 189–203, doi: 10.4133/JEEG1.3.189.

Ramirez, A., W. Daily, D. LaBrecque, E. Owen, and D. Chesnut, 1993, Monitoring an underground steam injection process using electrical-resistance tomography: Water Resources Research, **29**, 73–87, doi: 10.1029/92WR01608.

Ramirez, A. L., R. L. Newmark, and W. D. Daily, 2003, Monitoring carbon dioxide floods using electrical resistance tomography (ERT): Sensitivity studies: Journal of Environmental and Engineering Geophysics, **8**, no. 3, 187–208, doi: 10.4133/JEEG8.3.187.

Rücker, C., T. Günther, and K. Spitzer, 2006, Three-dimensional modelling and inversion of DC resistivity data incorporating topography I. Modeling: Geophysical Journal International, **166**, 495–505, doi: 10.1111/gji.2006.166.issue-2.

Sakurai, S., T. S. Ramakrishnan, A. Boyd, N. Mueller, and S. Hovorka, 2005, Monitoring saturation changes for CO_2 sequestration: Petrophysical support of the Frio brine pilot experiment: Presented at the 46th Annual Logging Symposium Transactions, SPWLA.

Schilling, F. R., G. Borm, H. Würdemann, F. Möller, and M. Kühn, CO_2SINK Group, 2009, Status report on the first European on-shore CO_2 storage site at Ketzin (Germany): Energy Procedia, **1**, 2029–2035.

Schmidt-Hattenberger, C., P. Bergmann, D. Kiessling, K. Krüger, C. Rücker, and H. Schütt, CO_2SINK Group, 2011, Application of a vertical electrical resistivity array (VERA) for monitoring CO_2 migration at the Ketzin site: First performance evaluation: Energy Procedia, **4**, 3363–3370.

Schmidt-Hattenberger, C., P. Bergmann, T. Labitzke, S. Schröder, K. Krüger, C. Rücker, and H. Schütt, 2012, A modular geoelectrical monitoring system as part of the surveillance concept in CO_2 storage projects: Energy Procedia, **23**, 400–407, doi: 10.1016/j.egypro.2012.06.062.

Schütt, H., M. Wigand, and E. Spangenberg, 2005, Geophysical and geochemical effects of supercritical CO_2 on sandstones, *in* D. C. Thomas, and S. Benson, eds., Carbon dioxide capture for storage in deep geologic formations-results from the CO_2 capture project: Elsevier, 767–786, doi: 10.1016/B978-008044570-0/50133-1.

Schütze, C., and Ch. Flechsig, 2002, Structural investigation of an active hydrothermal system beneath the Long Valley Caldera, California, using DC-resistivity imaging methods: Zeitschrift für Geologische Wissenschaften, **30**, 119–129.

Si, H., 2003, TETGEN: A 3D delaunay tetrahedral mesh generator, http://tetgen.berlios.de, accessed 01 December 2010.

Slater, L., A. M. Binley, W. Daily, and R. Johnson, 2000, Crosshole electrical imaging of a controlled saline tracer injection: Journal of Applied Geophysics, **44**, no. 2–3, 85–102, doi: 10.1016/S0926-9851(00)00002-1.

Storz, H., W. Storz, and F. Jacobs, 2000, Electrical resistivity tomography to investigate geological structures of the earth's upper crust: Geophysical Prospecting, **48**, 455–471, doi: 10.1046/j.1365-2478.2000.00196.x.

Streich, R., M. Becken, U. Matzander, and O. Ritter, 2011, Strategies for land-based controlled-source electromagnetic surveying in high-noise regions: The Leading Edge, **30**, 1174–1181, doi: 10.1190/1.3657078.

Wiese, B., J. Böhner, C. Enachescu, H. Würdemann, and G. Zimmermann, 2010, Hydraulic characterisation of the Stuttgart Formation at the pilot test site for CO_2 storage, Ketzin, Germany: International Journal of Greenhouse Gas Control, **4**, 960–971, doi: 10.1016/j.ijggc.2010.06.013.

Würdemann, H., F. Möller, M. Kühn, G. Borm, and F. Schilling, CO_2SINK-Group, 2010, The field-laboratory for CO_2 storage "CO_2SINK" at Ketzin (Germany): Site preparation, baseline surveys and the first year of operation: International Journal of Greenhouse Gas Control, **4**, 938–951.

Xue, Z., J. Kim, S. Mito, K. Kitamura, and T. Matsuoka, 2009, Detecting and monitoring CO_2 with P-wave velocity and resistivity from both laboratory and field scales: SPE International Conference on CO2 Capture, Storage and Utilization, SPE 126885.

Zemke, K., A. Liebscher, and M. Wandrey, CO_2SINK Group, 2010, Petrophysical analysis to investigate the effects of carbon dioxide storage in a subsurface saline aquifer at Ketzin, Germany (CO_2SINK): International Journal of Greenhouse Gas Control, **4**, 990–999, doi: 10.1016/j.ijggc.2010.04.008.

Zimmer, M., J. Erzinger, and C. Kujawa, CO_2SINK-Group, 2011, The gas membrane sensor (GMS): A new method for gas measurements in deep boreholes applied at the CO_2SINK site: International Journal of Greenhouse Gas Control, **5**, 995–1001, doi: 10/1016/j/ijggc.2010.11.007.